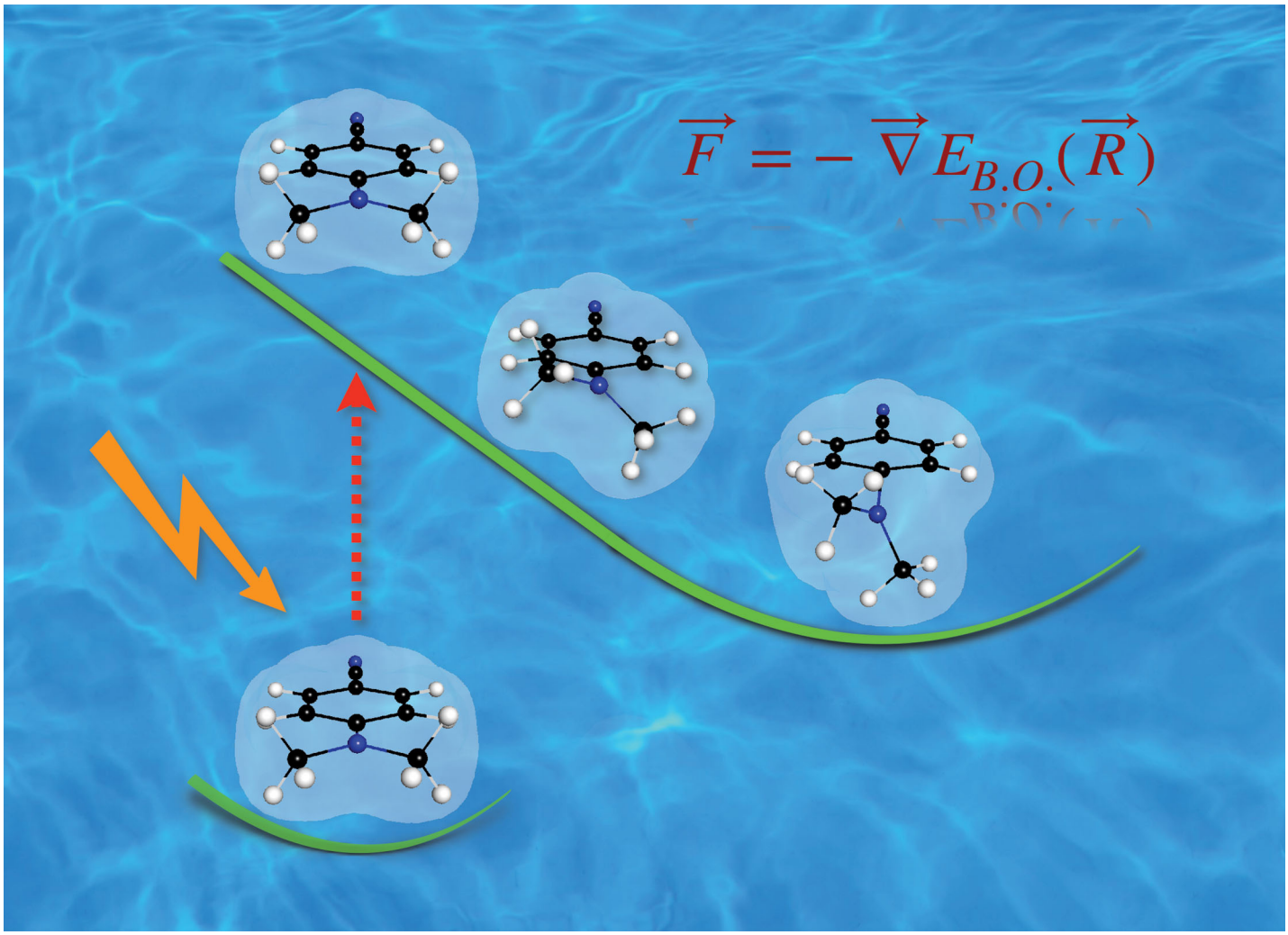


Showcasing research from the Quantum Chemistry Group of Prof. Dr Christof Hättig at Ruhr-Universität Bochum, Germany

COSMO-RI-ADC(2) excitation energies and excited state gradients

This work reports an implementation of analytic gradients for electronically excited states for the correlated wavefunction method ADC(2) in combination with the COSMO polarizable continuum model as an implicit solvent model. The coupling of COSMO and ADC(2) in the framework of the post-SCF reaction field scheme provides an appropriate tool to study solvent effects on excited state relaxation dynamics, equilibrium geometries and potential energy surfaces for both equilibrium and non-equilibrium situations.

As featured in:



See Sarah Karbalaei Khani *et al.*, *Phys. Chem. Chem. Phys.*, 2018, **20**, 16354.

ROYAL SOCIETY OF CHEMISTRY

rsc.li/pccp

Registered charity number: 207890

PCCP

PAPER

View Article Online
View Journal | View Issue

Check for updates

Cite this: *Phys. Chem. Chem. Phys.*, 2018, **20**, 16354

COSMO-RI-ADC(2) excitation energies and excited state gradients†

Sarah Karbalaei Khani, * Alireza Marefat Khah and Christof Hättig

Received 29th January 2018,
Accepted 19th April 2018

DOI: 10.1039/c8cp00643a

rsc.li/pccp

We present an implementation of analytic gradients for electronically excited states for the algebraic-diagrammatic construction through second order, ADC(2), in combination with the conductor-like screening model (COSMO) as an implicit solvent model. The implementation uses a post-SCF reaction field scheme for the coupling between the environment and the quantum system which retains the computational efficiency of the gas-phase RI-ADC(2) calculations. Applying this approach, we computed solvatochromic shifts for UV absorption and fluorescence transitions of 4-(*N*,*N*-dimethylamino)benzonitrile using equilibrium geometries for the ground and the first excited states optimized in the presence of acetonitrile as solvent. Furthermore, we investigated the excited state energies and geometries of the 2-iodobenzimidazolium·triflate ion pair in aqueous solution as an example where solvent effects have a large influence on the structure and the UV spectrum.

Published on 20 April 2018. Downloaded by Ruhr Universitat Bochum on 1/16/2019 9:37:32 AM.

1 Introduction

The inclusion of solvent effects not only on the absorption and emission processes but also on the geometrical structure in ground and excited states are essential for a detailed understanding of the photophysics and photochemistry of molecular systems in solution. A potentially very accurate strategy to compute excitation energies of molecules in solution consists of the inclusion of a large number of explicit solvent molecules combined with a sampling over a statistically representative number of configurations to reproduce bulk and fluctuation effects. However, if this approach is used with accurate quantum mechanical (QM) methods the sampling triggers even for a relatively small number of explicit solvent molecules high computational costs.

The main effects of solute–solvent interactions on electronic excitations are generally of electrostatic origin and related to the solvent polarity. The importance of elucidating these electrostatic effects using a computationally affordable approach gave rise to the formulation of continuum solvation models (CSMs) which use an implicit average description of solute–solvent interactions and are nowadays widely used in combination with different quantum chemical methods.[1–4] One of the most popular CSM approaches used in combination with electronic spectra is the Polarizable Continuum Model (PCM)[5] in different parameterizations.[6] The PCM model has been implemented for excited state energies and analytic gradients in solution at the configuration interaction singles (CIS) level,[7] as well as for time-dependent density functional theory (TDDFT) and the coupled-cluster singles and doubles (CCSD) model.[8–13] In the context of QM continuum solvation or in general for QM reaction field methods, there exist different approaches to compute electronic excitation energies. Two of them are the state specific (SS) and the linear response (LR) approach. The state specific strategy solves the non-linear Schrödinger equations for the states of interest assuming that the excitation energies are the differences between the corresponding total solute–solvent free energies,[14,15] while the linear-response strategy avoids the explicit calculation of the excited state wave functions and computes the excitation energies as the poles of the linear response function using a common eigenvalue equation for all excited states.[16,17] For a QM system in vacuum the two approaches are equivalent as long as the equivalence is not broken by approximations in the wavefunction ansatz. This is no longer true for a QM system embedded in a polarizable environment (reaction field), where the partitioning of the full system into separately treated subsystems—the QM system and the environment—coupled by a wavefunction- or density-dependent interaction leads to a non-linear Schrödinger equation. In this case the SS and LR approaches differ from the onset unless the full supermolecular solution is recovered. Both approaches along with a corrected LR (cLR) approach to reduce the gap between the SS and LR formalisms have been used *e.g.* within the TDDFT framework.[18–21] In the context of reaction field schemes for correlated wavefunction methods these issues have been reviewed at the example of COSMO-ADC(2) by Lunkenheimer and Köhn.[22]

Arbeitsgruppe Quantenchemie, Ruhr-Universität, Bochum 44780, Germany. E-mail: Sarah.KarbalaeiKhani@rub.de, Alireza.MarefatKhah@rub.de, Christof.Haettig@rub.de

† Electronic supplementary information (ESI) available. See DOI: 10.1039/c8cp00643a

This journal is © the Owner Societies 2018

Published on 20 April 2018. Downloaded by Ruhr Universitat Bochum on 1/16/2019 9:37:32 AM.

Implementations of PCM for excitation energies have also been reported for coupled-cluster (CC) methods which can provide more accurate results than TDDFT especially for charge-transfer transitions. For correlated wavefunction methods that use orbitals from preceding *e.g.* Hartree–Fock (HF) calculations and do not optimize them simultaneously with the correlated wavefunction, the non-linearity of the Schrödinger equation for a QM system in a reaction field produces complications already for the ground state. Among different approaches proposed to deal with this problem in an approximate manner in CC and other correlated wavefunction methods,[23,24] there are two approximations called PTED (perturbation theory with self-consistent energy and density) and PTE, using the HF reaction field. The latter scheme neglects post-Hartree–Fock contributions to the reaction field and introduces solute–solvent interactions only through the Fock operator and the polarization of the molecular orbitals (MOs) while the former scheme (PTED) is considered to be a more complete form in which the correlated electronic density is used to calculate a self-consistent reaction field. Beside the aforementioned schemes, two intermediate approximations between PTE and PTED called PTE(S) and PTES (where S stands for singles) have been proposed for CCSD by Caricato[25] to calculate free energies and analytic gradients to improve upon the PTE approximation towards the PTED results with less computational efforts than the latter. However, CCSD often gives molecular structures that are not very accurate and is computationally expensive.

The conductor-like screening model (COSMO)[26] is another extensively used CSM which shares many features with PCM, in particular with the C-PCM variant of the latter. COSMO has been implemented by Lunkenheimer and Köhn[22] for electronic excitation energies with the ADC(2) (algebraic diagrammatic construction through second-order)[27] method, which is based on second-order Møller–Plesset perturbation theory, in the ricc2[28] module of TURBOMOLE.[29,30] For long-lived states (the ground state or the lowest excited states) this implementation applies SS approaches and the reaction field is calculated fully self-consistently in an iterative PTED scheme. For short-lived states where only the fast part of the reaction field can respond to the changes in the electron density a cLR scheme is adopted, based on the PTED reaction field of the reference state. Although PTED is in certain aspects the most complete scheme, its high computational costs for post-HF and post-KS methods as well as the complication to extend it for analytic gradients make it a less preferred choice.

In the current work we report an implementation of COSMO-ADC(2) with a reaction field scheme that was originally developed in the context of the PERI-CC2[31] method (where PE stands for polarizable embedding) as an approach that is an intermediate between PTE and PTED. This scheme, which we will denote in the following as post-SCF, has some similarities to the PTES scheme proposed by Caricato,[25] but was especially designed to compute electronic excitation energies and other response properties in solution in such a way that it retains the computational efficiency of the vacuum RI-CC2 or RI-ADC(2) methods while capturing all important solvent effects on excited state energies at the LR level of the correlated wavefunction.[31] This reaction field scheme allows for a straight-forward implementation of the corresponding analytic gradients for the excited state energies which we report in the current work for COSMO-RI-ADC(2). It avoids the self-consistent iterations of the PTED scheme around the Hartree–Fock and post-HF calculations as well as the accompanied danger of numerical instabilities if the reaction field is not converged tightly enough. As long as no state-specific corrections are included, it provides excited state potential energy surfaces (PES) with a consistent behavior at avoided crossings and conical intersections.

2 Theory

2.1 The conductor-like screening model

The dielectric continuum approach assumes the solvent as a structureless continuum in which the solute is surrounded by a molecule-shaped cavity. The cavity is discretized into small surface segments. COSMO is an apparent surface charge (ASC) model with polarized charges created by the mutual polarization of the solvent and the solute which are spread on the cavity surface.[26] In the COSMO picture of isotropic solution, the solvent reaction field is obtained as an integral over the surface charge distribution which in the actual implementation is represented by point charges placed at the centers of the cavity surface segments. The free energy $\mathscr{G}$ of the solute embedded in a dielectric continuum is within the COSMO model in an equilibrium situation given by:

$$\mathscr{G} = \langle \hat{H}^{\mathrm{QM}} \rangle - \frac{1}{2} f(\varepsilon) \sum_{\mu\nu} V_\mu \left[\mathscr{A}^{-1}\right]_{\mu\nu} V_\nu. \tag{1}$$

In the above equation $\mathscr{A}$ is the response kernel for COSMO,[26] $f(\varepsilon)$ a scaling factor depending on the dielectric constant of the solvent ε and V_μ the value of the electrostatic potential at the center of the surface segment μ which is given by:

$$V_\mu = \left\langle \frac{\hat{Q}(\mathbf{r})}{|\mathbf{t}_\mu - r|} \right\rangle, \tag{2}$$

where $\mathbf{t}_\mu$ is the center of segment μ and $\hat{Q}(\mathbf{r})$ the charge density operator. The angle brackets $\langle\,\rangle$ denote the quantum mechanical expectation value. The polarization charges induced by the solute on the cavity segments are obtained as:

$$Q_\mu = -f(\varepsilon) \sum_{\nu} \left[\mathscr{A}^{-1}\right]_{\mu\nu} V_\nu. \tag{3}$$

2.2 ADC(2) and its relation to CC2

The second order methods CIS(D),[32] CC2[33] and ADC(2)[27] provide excitation energies for singly excited states with similar accuracy as those obtained with the computationally more demanding CCSD method. The non-perturbative CC2 and ADC(2) methods are also found to give equilibrium structures and vibrational frequencies which for main group single-reference molecules usually are superior to those from CCSD which is, however, more robust with respect to strong correlation effect.[34] An advantage of ADC(2) over CC2 for excited state calculations is that for ADC(2) the excitation energies are obtained as the eigenvalues of

Published on 20 April 2018. Downloaded by Ruhr Universitat Bochum on 1/16/2019 9:37:32 AM.

a Hermitian secular matrix[34] while in coupled-cluster response theory the excitation energies are computed as eigenvalues of a non-Hermitian Jacobi matrix.[28] This guarantees for ADC(2) a qualitatively correct description of conical intersections between states of the same symmetry. In addition, it reduces the computational costs for analytic gradients by almost a factor of four since no separate equations need to be solved for left and right eigenvectors and the first-order ground state amplitudes and the corresponding Lagrange multipliers can in a canonical basis be calculated without solving coupled equations.

In contrast to the CC2 model,[33] ADC(2) is not derived from the response function of a ground state method. Therefore, there is no unique definition of the total energy for it. To be consistent with the order to which correlation effects are included as well as for computational convenience, second order Møller–Plesset perturbation (MP2) theory is applied to define the ground state energy. From technical and practical points of view ADC(2) and CC2 are, however, very similar. If we consider the CC2 Jacobi matrix as a function of the ground state singles and doubles amplitudes, $\mathbf{A}(T_1,T_2)$, its relation to the secular matrix of the ADC(2) model can be expressed as[34]

$$\mathbf{A}^{\mathrm{ADC(2)}} = \frac{1}{2}\left(\mathbf{A}\left(0, T_2^{\mathrm{MP1}}\right) + \mathbf{A}\left(0, T_2^{\mathrm{MP1}}\right)^{\dagger}\right) \tag{4}$$

where the CC2 cluster amplitudes are replaced by those from first-order perturbation theory and only the Hermitian part of the matrix is included.

2.3 COSMO-ADC(2) with the post-SCF coupling scheme

As pointed out in the introduction, for correlated wavefunction methods or in general for post-SCF methods, there are different possibilities to couple the QM system to the environment for the reaction field calculation:

• The perturbation at the energy (PTE) scheme uses the reaction field obtained from the ground state HF density. The disadvantage of this scheme is that the environment does not respond to electronic excitation processes in the QM system and therefore important contributions for the coupling between the excitation process in the QM system and the reaction field are missing if the QM system is not chosen large enough. The computational costs for this scheme are comparable to those for the corresponding gas-phase calculations.

• The perturbation at the energy and density (PTED) scheme is the most expensive one. It makes the post-HF density and the solvent reaction field self-consistent; usually in a loop over the HF and the post-HF calculation which is terminated once the remaining changes are below certain thresholds. The PTED scheme has already been implemented for COSMO-MP2 and COSMO-ADC(2) in the TURBOMOLE[22,29,30] package. However, it is not the method of choice for potential energy surfaces because of the dependence of the excited state energies on the choice of the reference state for the reaction field. The state-specific reaction field contributions lead to a qualitatively wrong behavior of the excited state potential energy surfaces in the vicinity of near degeneracies and state intersection. Furthermore, the self-consistency iterations lead to high computational costs and can affect the numerical stability of geometry optimizations if the convergence thresholds are not tight enough. These issues motivated us to apply an alternative scheme for the coupling between the reaction field and the solute.

• The post-SCF scheme that we implemented for COSMO-RI-CC2 excitation energies and COSMO-RI-ADC(2) excitation energies and excited state gradients evaluates the post-HF contributions to the solvent reaction field with an approximate post-HF contribution to the density, ($\mathbf{D}^{\Delta}$), which is calculated only from the single excitation parts of the cluster amplitudes, Lagrange multipliers or eigenvectors. This scheme has already been applied for the implementation of PERI-CC2 excitation energies, and one- and two-photon transition moments.[31,35] The computational costs of this scheme are comparable to the corresponding gas-phase calculations and the energies for all excited states are obtained from a single eigenvalue equation so that the obtained potential energy surfaces show a consistent behavior at avoided crossings and conical intersections.

Furthermore, for excited state one can combine the linear response approach with state-specific perturbative corrections to account for the response of the reaction field to the difference between the ground and the excited state charge density (see *e.g.* ref. 22 for a related discussion at the COSMO-ADC(2) level). While from a practical point of view, perturbative state-specific corrections are very useful for computing excitation energies for given structures, they are very problematic for excited state geometry optimizations. As all non-degenerate perturbation theories (for example CIS(D)), such state-specific corrections will again lead to potential energy surfaces (PES) which behave qualitatively wrong in the vicinity of near degeneracies and intersections. Since the latter are ubiquitous in polyatomic molecules, perturbative methods are usually not applicable for studying their excited state PES.

The post-SCF scheme used for RI-CC2 and RI-ADC(2) can be derived from the general free energy Lagrangian for the full CC model in a self-consistent reaction field framework as:[36]

$$L_{\text{COSMO-CC}}(t,\bar{t}) = \left\langle \Lambda \middle| \hat{H}^{\mathrm{QM}} \middle| \mathrm{CC} \right\rangle + \frac{1}{2}\sum_{\kappa\lambda} Q_{\kappa}\left(\mathbf{D}^{\mathrm{CC}}\right) V_{\lambda}\left(\mathbf{D}^{\mathrm{CC}}\right) \tag{5}$$

$$= \left\langle \Lambda \middle| \hat{H}^{\mathrm{QM}} + \frac{1}{2}\hat{G}^{\mathrm{pol}} \middle| \mathrm{CC} \right\rangle \tag{6}$$

where the Λ state is defined as

$$\langle \Lambda| = \left(\langle \mathrm{HF}| + \sum_{\mu_i}\sum_{i} \bar{t}_{\mu_i}\langle \mu_i|\right)\exp(-\hat{T}). \tag{7}$$

In eqn (5) and (6), $\hat{H}^{\mathrm{QM}}$ is the vacuum electronic Hamiltonian, $\hat{G}^{\mathrm{pol}}$ is the electronic interaction operator between the QM system and the reaction field—in the case of COSMO with the cavity surface charges—and $\mathbf{D}^{\mathrm{CC}}$ is the unrelaxed CC density which is defined as

$$\mathbf{D}^{\mathrm{CC}}_{pq} = \langle \Lambda | \hat{E}_{pq} | \mathrm{CC} \rangle \tag{8}$$

 This journal is © the Owner Societies 2018

Published on 20 April 2018. Downloaded by Ruhr Universitat Bochum on 1/16/2019 9:37:32 AM.

where $\hat{E}_{pq}$ are the spin-free one-particle operators. For implicit solvent models, like PCM and COSMO, the different time scales for the relaxation of the nuclear and the electronic polarization of the environment should be taken into account by replacing $f(\varepsilon)$ (see eqn (1)) by a frequency-dependent factor. Also in the current implementation we allow that f is chosen as a step function which in the static limit and at low frequencies (*i.e.* equilibrium situations) is defined as $f(\varepsilon)$, where ε is the static dielectric constant while in the optical range it changes to $f(n^2)$ where n is the refractive index.

From the general ansatz introduced in eqn (6) the corresponding free energy Lagrangian for the CC2 model is derived by skipping all contributions beyond second order in the fluctuation potential, but counting the singles amplitudes as zeroth-order because of their special role in response theory:

$$\begin{aligned} L = \mathscr{G}_{\mathrm{HF}} &+ \left\langle \mathrm{HF}\middle|\hat{\tilde{F}}_{\mathrm{N}}^{\mathrm{pol}} + \hat{\tilde{W}}_{\mathrm{N}}^{\mathrm{QM}} + \left[\hat{\tilde{W}}_{\mathrm{N}}^{\mathrm{QM}}, \hat{T}_2\right] + \frac{1}{2}\hat{\tilde{G}}(\mathbf{D}^{\Delta})\middle|\mathrm{HF}\right\rangle \\ &+ \left\langle \bar{t}_1\middle|\hat{\tilde{F}}_{\mathrm{N}}^{\mathrm{pol}} + \hat{\tilde{W}}_{\mathrm{N}}^{\mathrm{QM}} + \left[\hat{F}_{\mathrm{N}}^{\mathrm{pol}} + \hat{\tilde{W}}_{\mathrm{N}}^{\mathrm{QM}}, \hat{T}_2\right]\middle|\mathrm{HF}\right\rangle \\ &+ \left\langle \bar{t}_2\middle|\left[\hat{F}_{\mathrm{N}}^{\mathrm{pol}}, \hat{T}_2\right] + \hat{\tilde{W}}_{\mathrm{N}}^{\mathrm{QM}}\middle|\mathrm{HF}\right\rangle. \end{aligned} \tag{9}$$

In the above equation operators are introduced in their normal ordered form with respect to the HF wave function.

$$\hat{O}_{\mathrm{N}} = \hat{O} - \langle \mathrm{HF}|\hat{O}|\mathrm{HF}\rangle \tag{10}$$

Furthermore, double excitation amplitudes and Lagrange multipliers are neglected for the density from which the post-HF contribution to the reaction field is calculated as:

$$\mathbf{D}^{\Delta}_{pq} = \langle \mathrm{HF} + \bar{t}_1|\mathrm{e}^{-\hat{T}_1}\hat{E}_{pq}\mathrm{e}^{\hat{T}_1}|\mathrm{HF}\rangle - \langle \mathrm{HF}|\hat{E}_{pq}|\mathrm{HF}\rangle. \tag{11}$$

In eqn (9) we introduced the Fock operator for the embedded system, $\hat{F}^{\mathrm{pol}} = \hat{F}^{\mathrm{QM}} + \hat{G}^{\mathrm{pol,HF}}$ and the fluctuation potential $\hat{W}^{\mathrm{QM}} = \hat{H}^{\mathrm{QM}} - \hat{F}^{\mathrm{QM}}$. With a tilde we denote operators dressed with the ground state singles amplitudes as $\hat{\tilde{O}} = \exp(-\hat{T}_1)\hat{O}\exp(\hat{T}_1)$. The density-dependent reaction field operators for COSMO are defined as:

$$\hat{G}(\mathbf{D}) = \sum_{\mu} Q_{\mu}(\mathbf{D}) V_{pq,\mu}\hat{E}_{pq}, \tag{12}$$

$$Q_{\mu}(\mathbf{D}) = -f\sum_{\nu}\left[\mathbf{A}^{-1}\right]_{\mu\nu}\sum_{pq} V_{pq,\nu}D_{pq}, \tag{13}$$

$$V_{pq,\nu} = -\left\langle p\middle|\frac{1}{|\mathbf{t}_{\nu} - \mathbf{r}|}\middle|q\right\rangle. \tag{14}$$

In eqn (13) the frequency-dependence of the reaction field polarization enters through $\hat{G}(\mathbf{D}^{\Delta})$ *via* the scaling factor f.

For COSMO-MP2, which is used as the ground state for COSMO-ADC(2), density $\mathbf{D}^{\Delta}$ vanishes if the Hartree–Fock wavefunction fulfills the Brillouin condition. Then the singles amplitudes t_{μ_1} and Lagrange multipliers $\bar{t}_{\mu_1}$ become zero in first-order perturbation theory so that the above approach reduces at the MP2 level to PTE-COSMO-MP2. The expressions for the polarization contributions to the CC2 Jacobian have been discussed for the atomistic polarizable embedding (PE) in ref. 31. Given those expressions along with the relation (4), the polarization contributions to the ADC(2) secular matrix are obtained as:

$$\mathbf{A}^{\mathrm{pol}}_{\mu_1,\nu_1} = \langle \mu_1|\left[\hat{G}^{\mathrm{pol,HF}}, \tau_{\nu_1}\right] + \hat{G}^{\nu_1}|\mathrm{HF}\rangle \tag{15}$$

$$\mathbf{A}^{\mathrm{pol}}_{\mu_1,\nu_2} = 0 \tag{16}$$

$$\mathbf{A}^{\mathrm{pol}}_{\mu_2,\nu_1} = 0 \tag{17}$$

$$\mathbf{A}^{\mathrm{pol}}_{\mu_2,\nu_2} = \langle \mu_2|\left[\hat{G}^{\mathrm{pol,HF}}, \tau_{\nu_2}\right]|\mathrm{HF}\rangle, \tag{18}$$

where

$$\hat{G}^{\mathrm{pol,HF}} = \sum_{\mu}\left\langle \mathrm{HF}|\hat{Q}_{\mu}|\mathrm{HF}\right\rangle \hat{V}_{\mu}. \tag{19}$$

The operator in the last term of eqn (15) for the singles-singles block $\mathbf{A}^{\mathrm{pol}}_{\mu_1\nu_1}$ is defined as the derivative of $\hat{G}(\mathbf{D}^{\Delta})$ with respect to the cluster amplitudes. Its contribution to the linear transformation of the secular matrix with a vector R_{ν} are evaluated through an auxiliary density $\mathbf{D}^{\eta}$ defined *via* the derivative of $\mathbf{D}^{\Delta}$ with respect to t_{ν_1}:

$$\mathbf{D}^{\eta} = \sum_{\nu_1}\frac{\partial \mathbf{D}^{\Delta}}{\partial t_{\nu_1}}R_{\nu_1}, \tag{20}$$

$$\sum_{\nu_1}\langle \mu_1|\hat{G}^{\nu_1}|\mathrm{HF}\rangle R_{\nu_1} = \langle \mu_1|\hat{G}(\mathbf{D}^{\eta})|\mathrm{HF}\rangle. \tag{21}$$

In the same way, its contribution to left transformations are evaluated as:

$$\sum_{\mu_1} L_{\mu_1}\langle \mu_1|\hat{G}^{\nu_1}|\mathrm{HF}\rangle = \langle \mathrm{HF}|\left[\hat{G}(\mathbf{D}^{\xi}), \tau_{\mu_1}\right]|\mathrm{HF}\rangle \tag{22}$$

with the auxiliary density

$$\mathbf{D}^{\xi} = \sum_{\mu_1} L_{\mu_1}\frac{\partial \mathbf{D}^{\Delta}}{\partial \bar{t}_{\mu_1}}. \tag{23}$$

For CC2, the auxiliary transition densities $\mathbf{D}^{\eta}$ and $\mathbf{D}^{\xi}$ differ in terms that depend on t_1 and $\bar{t}_1$ while for ADC(2) the difference reduces to a factor of 2 from spin summation in the spin-free closed shell case when a biorthonormal basis for the single excitation manifold with $|ck\rangle = \hat{E}_{ck}|\mathrm{HF}\rangle$ and $\langle ck| = \frac{1}{2}\langle \mathrm{HF}|\hat{E}^{\dagger}_{ck}$ is used. In the non-equilibrium limit, *i.e.* for vertical electronic transitions and for short time scales after the transition, $\hat{G}(\mathbf{D}^{\eta})$ and $\hat{G}(\mathbf{D}^{\xi})$ should be evaluated with $f(n^2)$, while in equilibrium situations, *i.e.* for time scales long compared to the solvent relaxation time, they should be evaluated with $f(\varepsilon)$.

2.4 Excited state gradient theory for COSMO-RI-ADC(2)

As pointed out above, ADC(2) technically differs from CC2 in two aspects: the ground state singles and doubles amplitudes $\hat{T}_1$ and $\hat{T}_2$ are those from first-order Møller–Plesset perturbation theory, where the ground state singles amplitudes $\hat{T}_1$ vanish if $|\mathrm{HF}\rangle$ fulfills the Brillouin condition. Furthermore, ADC(2) has a symmetric secular matrix in contrast to the non-hermitian CC2 Jacobian.

Published on 20 April 2018. Downloaded by Ruhr Universitat Bochum on 1/16/2019 9:37:32 AM.

2.4.1 The relaxed excited state Lagrange function. The orbital-relaxed Lagrange function for the total energy of an excited state f at the COSMO-RI-ADC(2) level of theory is formulated as:

$$\begin{aligned} L^{\mathrm{f}} &= \langle \mathrm{HF}|\hat{F}^{\mathrm{QM}} + \hat{W}^{\mathrm{QM}} + [\hat{W}^{\mathrm{QM}}, \hat{T}_2]|\mathrm{HF}\rangle \\ &+ \sum_{\mu_2} \bar{t}^{\mathrm{f}}_{\mu_2} \langle \mu_2|[\hat{F}^{\mathrm{pol}}, \hat{T}_2] + \hat{W}^{\mathrm{QM}}|\mathrm{HF}\rangle \\ &+ \sum_{i,j=1}^{2} \sum_{\mu_i\nu_j} \bar{E}^{\mathrm{f}}_{\mu_i} A_{\mu_i\nu_j} E^{\mathrm{f}}_{\nu_j} + \bar{\omega}^{\mathrm{f}} \left(1 - \sum_{i=1}^{2} \sum_{\mu_i} \bar{E}^{\mathrm{f}}_{\mu_i} E^{\mathrm{f}}_{\mu_i}\right) \\ &+ \frac{1}{2} \sum_{\mu} \left\langle \mathrm{HF}|\hat{Q}_\mu|\mathrm{HF}\right\rangle \langle \mathrm{HF}|\hat{V}_\mu|\mathrm{HF}\rangle + \sum_{\mu_0} \bar{\kappa}_{\mu_0} F^{\mathrm{pol}}_{\mu_0}. \end{aligned} \tag{24}$$

The first term in eqn (24) represents the HF and MP2 ground state energy, the second term accounts for the first order amplitude equations for $\hat{T}_2$ and the third term gives the excitation energy. $\bar{E}^{\mathrm{f}}$ and E^{f} are formally the left and right eigenvectors of **A** (for ADC(2) they are equivalent). The fourth term accounts for the normalization of the eigenvectors and the sixth term for the Hartree–Fock equations. The fifth term represents the polarization energy for the HF ground state. Thus, explicit effects of the polarizable continuum environment on the electronic excited states enter in the Lagrange function through the secular matrix **A**, the Fock matrix $\mathbf{F}^{\mathrm{pol}}$ and the HF polarization energy.

Requiring the Lagrangian to be stationary with respect to variations of the amplitudes t_{μ_2} gives the equations for the Lagrange multipliers $\bar{t}_{\mu_2}$:

$$\begin{aligned} \frac{\mathrm{d}L^{\mathrm{f}}}{\mathrm{d}t^{\mathrm{f}}_{\mu_2}} &= \langle \mathrm{HF}|[\hat{W}^{\mathrm{QM}}, \tau_{\mu_2}]|\mathrm{HF}\rangle + \langle E_1|[[\hat{W}^{\mathrm{QM}}, E_1], \tau_{\mu_2}]|\mathrm{HF}\rangle \\ &+ \left\langle \bar{t}^{\mathrm{f}}_{\mu_2}|[\hat{F}^{\mathrm{pol}}, \tau_{\mu_2}]|\mathrm{HF}\right\rangle = 0, \end{aligned} \tag{25}$$

which in a canonical MO basis can be directly inverted (cmp. ref. 34). In the same way, requiring stationarity with respect to orbital variations leads to the CPHF (or Z-vector) equations:

$$\sum_{AI} \bar{\kappa}_{AI} \left(A^{\kappa}_{AIBJ} - \delta_{AB}\varepsilon_A - \delta_{IJ}\varepsilon_I\right) = -\eta^{\kappa,\mathrm{f}}_{BJ}. \tag{26}$$

The capital indices refer to both active and frozen orbitals and ε_{p} are the orbital energies. The matrix A^{κ} on the left-hand side of eqn (26) is for COSMO defined as:

$$\begin{aligned} A^{\kappa}_{pqrs} &= \left\langle \mathrm{HF}\left|\left[\left[\hat{W}^{\mathrm{QM}}, E^{-}_{pq}\right], E^{-}_{rs}\right]\right|\mathrm{HF}\right\rangle \\ &+ \sum_{\mu} \left\langle \mathrm{HF}\left|\left[\hat{Q}_\mu, E^{-}_{pq}\right]\right|\mathrm{HF}\right\rangle \langle \mathrm{HF}|[\hat{V}_\mu, E^{-}_{rs}]|\mathrm{HF}\rangle. \end{aligned} \tag{27}$$

The expression for the right-hand-side (RHS) vector $\eta^{\kappa,\mathrm{f}}_{BJ}$ will be discussed below.

2.4.2 Excited state relaxed one- and two-electron densities. Our implementation of COSMO-RI-ADC(2) exploits the resolution of the identity (RI) approximation which allows for a fast atomic orbital (AO) to molecular orbital (MO) transformation at the level of three-index integrals and subsequent fast formation of the four-index integrals in the MO basis. The HF calculations can be done with or without applying the RI approximation. Therefore, we distinguish in the following between exact four-index integrals, $(pq|rs)$, from the HF energy and the Fock matrix and four-index integrals in the post-HF part which are always calculated within the RI approximation $(pq|rs)^{\mathrm{RI}}$.

Since we distinguished above between the charge density that couples the reaction field to the QM system and the exact charge density of the QM system, we obtain no explicit polarization contribution to the expression for the post-HF contributions to the (normal) one- and two-electron densities. Detailed expressions for the one-electron and the non-separable two-electron densities, $\mathbf{D}^{\mathrm{F,ex}}$ and $\mathbf{d}^{\mathrm{nsep,ex}}_{pqrs}$, that are used for the RI-ADC(2) gradients are given in ref. 34 and will not be repeated here. With them the RHS vector $\eta^{\kappa,\mathrm{f}}_{BJ}$ for COSMO-RI-ADC(2) can be calculated as:

$$\begin{aligned} \eta^{\kappa,\mathrm{f}}_{AI} &= \frac{1}{2}\left(D^{\mathrm{F,ex}}_{AI} + D^{\mathrm{F,ex}}_{IA}\right)(\varepsilon_I - \varepsilon_A) - \frac{1}{4}\sum_{pq}\left(D^{\mathrm{F,ex}}_{pq} + D^{\mathrm{F,ex}}_{qp}\right)A_{pqAI} \\ &+ \sum_{prs}\Big[\left(d^{\mathrm{nsep,ex}}_{pArs} + d^{\mathrm{nsep,ex}}_{Aprs}\right)(pI|rs)^{\mathrm{RI}} \\ &- \left(d^{\mathrm{nsep,ex}}_{pIrs} + d^{\mathrm{nsep,ex}}_{Iprs}\right)(Ap|rs)^{\mathrm{RI}}\Big] \\ &+ 2\sum_{i}\Big[G_{Ai}(\mathbf{D}^{\eta}(E_1))\left(D^{\xi}_{iI}(E_1) + D^{\xi}_{Ii}(E_1)\right) \\ &- G_{Ii}(\mathbf{D}^{\eta}(E_1))\left(D^{\xi}_{iA}(E_1) + D^{\xi}_{Ai}(E_1)\right)\Big]. \end{aligned} \tag{28}$$

After solution of the CPHF equations the gradients for the excited state can be evaluated as:

$$\begin{aligned} \frac{\mathrm{d}L}{\mathrm{d}x} &= \sum_{\alpha\beta} D^{\mathrm{eff,ao}}_{\alpha\beta} h^{[x]}_{\alpha\beta} + \frac{1}{2}\sum_{\alpha\beta\gamma\delta} d^{\mathrm{sep,ao}}_{\alpha\beta\gamma\delta}(\alpha\beta|\gamma\delta)^{[x]} \\ &- \sum_{\alpha\beta} F^{\mathrm{eff,ao}}_{\alpha\beta} S^{[x]}_{\alpha\beta} + \sum_{\alpha\beta P} \Lambda^{\mathrm{ao},P}_{\alpha\beta}(\alpha\beta|P)^{[x]} \\ &- \sum_{PQ} \gamma_{PQ} V^{[x]}_{PQ} + \frac{\mathrm{d}\Delta L^{\mathrm{pol,ex}}}{\mathrm{d}x}. \end{aligned} \tag{29}$$

We refer again to ref. 34 for detailed expressions of the AO and auxiliary densities. In the non-equlibrium limit the matrix $G(\mathbf{D}^{\eta})$ has to be computed with the screening function $f(n^2)$ for the optical range.

The explicit contributions from the reaction field to the analytic first derivatives of the excited state energy with respect to an external parameter x is:

$$\begin{aligned} \frac{\mathrm{d}\Delta L^{\mathrm{pol,ex}}}{\mathrm{d}x} &= \sum_{\kappa} Q^{\mathrm{HF}}_{\kappa}\left(\sum_{pq} D^{\mathrm{eff}}_{pq} V^{[x]}_{pq,\kappa} + V^{\mathrm{nuc},[x]}_{\kappa}\right) \\ &+ \sum_{\kappa}\left(Q^{\mathrm{eff}}_{\kappa} - Q^{\mathrm{HF}}_{\kappa}\right)\left(\sum_{pq} D^{\mathrm{HF}}_{pq} V^{[x]}_{pq,\kappa} + V^{\mathrm{nuc},[x]}_{\kappa}\right) \\ &+ \frac{1}{f(\varepsilon)}\sum_{\kappa\lambda} Q^{\mathrm{HF}}_{\kappa} \mathcal{A}^{[x]}_{\kappa\lambda}\left(Q^{\mathrm{eff}}_{\lambda} - \frac{1}{2}Q^{\mathrm{HF}}_{\lambda}\right) \\ &+ \sum_{\kappa\lambda} Q^{\xi}_{\kappa}\sum_{pq} D^{\eta}_{pq} V^{[x]}_{pq,\lambda} + \sum_{\kappa\lambda} Q^{\eta}_{\kappa}\sum_{pq} D^{\xi}_{pq} V^{[x]}_{pq,\lambda} \\ &+ \frac{1}{f(\varepsilon)}\sum_{\kappa\lambda} Q^{\xi}_{\kappa} \mathcal{A}^{[x]}_{\kappa\lambda} Q^{\eta}_{\lambda}. \end{aligned} \tag{30}$$

This journal is © the Owner Societies 2018

Published on 20 April 2018. Downloaded by Ruhr Universitat Bochum on 1/16/2019 9:37:32 AM.

In the last equation Q_κ^{HF}, Q_κ^ξ, Q_λ^η, and Q_κ^{eff} are the surface charges induced by the electron densities $\mathbf{D}^{HF}$, $\mathbf{D}^\xi$, $\mathbf{D}^\eta$, and $\mathbf{D}^{eff}$, respectively. For ADC(2) the contributions from Q_κ^η and $\mathbf{D}^\xi$ and from Q_κ^ξ and $\mathbf{D}^\eta$ are identical so that only one needs to be evaluated if the other is multiplied by a factor of 2. For expression for $\mathbf{D}^{eff}$ we refer to ref. 34. $\mathscr{A}_{\kappa\lambda}^{[x]}$ is the derivative of the COSMO response kernel (cmp. (1)), $V_{pq,\kappa}^{[x]}$ are the derivatives of the potential energy integrals, and $V_\kappa^{nuc,[x]}$ the respective nuclear counterparts. Here, the charges Q_κ^ξ and Q_λ^η are in the non-equilibrium limit calculated with $f(n^2)$ and in the equilibrium limit with $f(\varepsilon)$.

The COSMO-RI-ADC(2) excitation energies and excited state gradients have been implemented in a development version of the ricc2[28] module of the TURBOMOLE package.[29]

3 Applications

In the current section we present as application of the implemented code described above solvatochromatic shifts of the UV and fluorescence spectra in two molecular systems where a qualitatively correct simultaneous description of charge transfer excitations and solvent effects is important. Their structures are shown in Fig. 1. The first one is 4-(*N*,*N*-dimethyl-amino)-benzonitrile (DMABN) and the second one the intermolecular complex formed by the 2-iodo-benzimidazolium cation with the triflate anion.

All ground state geometry optimizations have been done at the MP2/def2-TZVPP (vacuum) and/or COSMO-MP2/def2-TZVPP (solution) level of theory. The vertical excitation energies as well as the excited state geometry optimizations are calculated at the COSMO-RI-ADC(2) level with def2-TZVPP orbital[37] and auxiliary[38] basis sets and the corresponding effective core potential[37] for iodine. The frozen core approximation was applied with the $1s^2$ orbitals kept frozen for all C, O, and N atoms. For iodine, all orbitals were frozen up to and including the $4s^24p^6$ shell. The post-SCF reaction field scheme was applied to couple the QM system to the environment. Cartesian coordinates are provided as Supporting Information. All MP2 and ADC(2) calculations were done with the ricc2[28] module of the TURBOMOLE[29,30] package.

3.1 Solvatochromic shifts of vertical excitation energies

4-(*N*,*N*-Dimethylamino)benzonitrile (DMABN) is a paradigmatic example of a phenomenon called dual fluorescence, because depending on the experimental conditions, *e.g.* in a polar solvent, it fluoresces at two different energies. This organic donor–acceptor compound has been studied extensively by theoretical and computational groups over the last decades. It shows in addition to a band from a locally excited (LE) state, which dominates the fluorescence spectra of DMABN in both vacuum and polar solvents, a low-energy fluorescence band from a state termed intramolecular charge transfer (ICT) state, which is only observed in polar solvents.

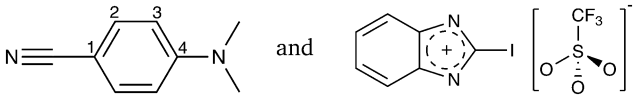


Fig. 1 Schematic structures of the investigated compounds.

Despite several computational studies on the spectroscopic properties of DMABN,[39–41] the solvent effects on the excited state energies and structures have not yet been investigated thoroughly at a correlated level of theory. In the following, we will discuss the excitation energies of DMABN at the ADC(2)/def2-TZVPP level in vacuum as well as in acetonitrile (non-equilibrium limit with ε = 36.7, n^2 = 1.81) as an example of a polar solvent, where we have used COSMO with both the PTED and the post-SCF reaction field schemes. Furthermore, we have used the gradient implementation for the post-SCF-COSMO-ADC(2)/def2-TZVPP approach to obtain the fully optimized equilibrium structure for the ICT state of DMABN in acetonitrile solution. Acetonitrile has been chosen as a solvent because a large amount of available computational and experimental data.[39,42–44]

According to ref. 45 and 46, the vertical excitations in vacuum and in the Franck–Condon region for the first excited state (LE) (also known as L_b state) is dominated by the one-electron HOMO → LUMO+1 transition and for the second excited state (ICT) (also known as L_a state) by the one-electron HOMO → LUMO transition. The results obtained for the vertical excitation energies, transition moments and excited state dipole moments in acetonitrile solution with COSMO-ADC(2) using the PTED and post-SCF reaction field schemes are listed together with the vacuum results in Table 1.

The PTED scheme predicts the second excited state as the bright state (f_2 = 0.63) and solvent induced shifts for the first and second excited state (LE and ICT, respectively) of −0.12 and −0.38 eV in acetonitrile, respectively. On the other hand, from the values for the oscillator strengths obtained with the post-SCF scheme we can conclude that this reaction field scheme predicts the bright state (f_2 = 0.71) to be the lowest excited state at 4.22 eV (with a solvatochromic shift of −0.46 eV). The analysis of the natural transition orbitals (NTOs) for the first two excited states,

Table 1 Calculated solvent shifts for the vertical excitation energies Δ^{sol} (eV), transition moments f and dipole moments μ (D) for the first two excited states of DMABN[a]

	Reaction field		
	In vacuo	PTED	Post-SCF
$\Delta\mathscr{G}_{1,0}$	4.42	4.29	4.31
$\Delta_{1,0}^{sol}$		−0.12	−0.11
f_1	0.03	0.03	0.05
μ_1	9.30	12.08	12.82
$\Delta\mathscr{G}_{2,0}$	4.69	4.30	4.22
$\Delta_{2,0}^{sol}$		−0.38	−0.46
f_2	0.55	0.63	0.71
μ_2	12.19	15.06	17.14

[a] All calculations are carried out at the COSMO-RI-ADC(2)/def2-TZVPP level using geometries optimized at the PTE-COSMO-MP2/def2-TZVPP level. Excited state energies are reported in different environments: '*in vacuo*' refers to the gas phase, for both PTED and post-SCF reaction field schemes acetonitrile has been used as the solvent (post-SCF reaction field has been used in the non-equilibrium solvation limit, ε = 36.7 and n^2 = 1.81). The PTED calculations are equilibrated for the ground state and include state-specific excited state non-equilibrium corrections.

Published on 20 April 2018. Downloaded by Ruhr Universitat Bochum on 1/16/2019 9:37:32 AM.

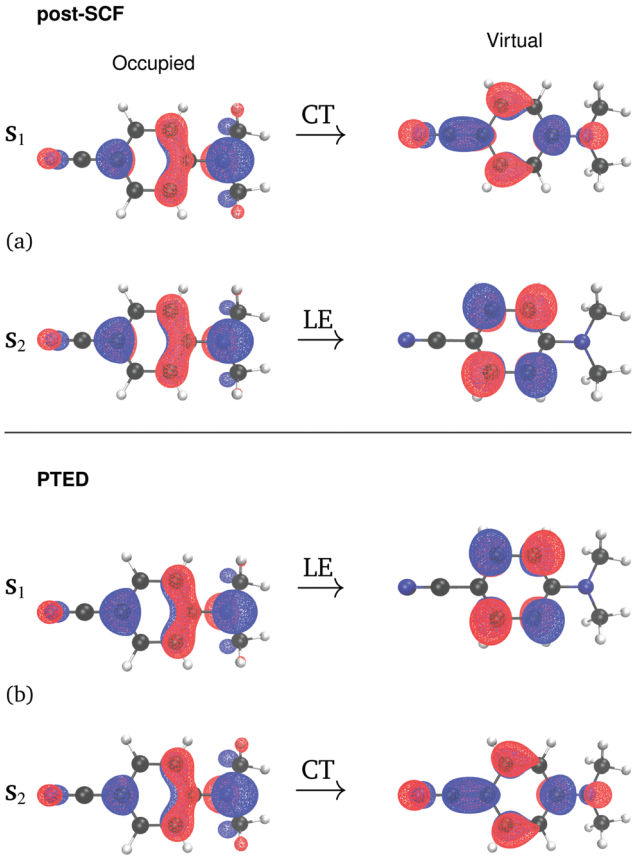


Fig. 2 Natural transition orbitals of DMABN calculated at the COSMO-ADC(2)/def2-TZVPP level in acetonitrile solution using (a) the post-SCF and (b) the PTED reaction field scheme.

Fig. 2, shows that S_1 and S_2 for the PTED scheme have LE and ICT characters, respectively, while for the post-SCF scheme the order is reversed. Table 1 shows that both schemes predict an increase of the dipole moments for both excited states with respect to the ground state (the ground state dipole moment in vacuum and solution are 7.41 and 9.94 D, respectively). The larger solvent shift for the L_a or ICT state in comparison to that for the L_b or LE state can be rationalized by the fact that the ICT state has a larger dipole moment (17.14 D with post-SCF and 15.06 D with PTED) compared to the LE state, and is thus more stabilized in a polar solvent like acetonitrile. An inversion of the order of the LE and ICT states in acetonitrile was also obtained by Scalmani[9] with PCM-TDDFT using a completely equilibrated response of the solvent for the calculation of vertical excitation energies.

With the post-SCF reaction field scheme the wall-time for the calculation of the vertical excitation energies plus the transition and dipole moments is very close to that of a corresponding calculation for the vacuum case and about five times shorter than for the PTED scheme.

To demonstrate the applicability of the developed COSMO-RI-ADC(2) excited state gradients to study the solvent effects on excited state structures, we studied the equilibrium geometry of the ICT state of DMABN in acetonitrile. According to the results reported in ref. 45, in the gas phase the LE state has a shallow

Table 2 Main geometrical parameters for the ground state (G.S.) and the ICT state in acetonitrile solution. The ground state geometry is optimized at the COSMO-MP2/def2-TZVPP and the excited ICT state at the COSMO-RI-ADC(2)/def2-TZVPP level (ε = 36.7, for the non-equilibrium limit n^2 = 1.81)

		ICT state		
	G.S.	COSMO eq.	COSMO non-eq.	Gas phase[a]
N–C_4[b]	1.36	1.42	1.42	1.44
C_3–C_4	1.42	1.44	1.44	1.45
C_2–C_3	1.38	1.37	1.37	1.37
C_1–C_2	1.40	1.44	1.44	1.43
C_1–C	1.42	1.40	1.40	1.41
C≡N	1.16	1.19	1.19	1.19
τ	0°	56°	65°	90°
ϕ	0°	32°	33°	41°

[a] Geometrical parameters of the ICT state with the C_s structure reported from ref. 45. [b] All the bond lengths are reported in Å. Atom numbers are the same as Fig. 1.

double minimum with a small twisting angle of $\tau = \pm 19°$ (τ is defined as the average of the dihedral angles $C_{Me}NC_4C_3$ and $C_{Me}'NC_4'C_3'$) with a small barrier of <0.05 eV. Some characteristic geometrical parameters of the ICT structures in acetonitrile solvent are collected in Table 2. Similar as in the gas phase studies,[45] the equilibrium geometry of the ICT state obtained at the RI-ADC(2)/def2-TZVPP level in acetonitrile solution, Fig. 3, has a twisted structure. The equilibrium geometry for the ICT state in the gas phase is found to have a twisted structure with a torsion angle of $\tau = 90°$ and an out-of-plane angle of $\phi = 41°$ (ϕ is defined as the angle of the C_4N bond with respect to a plane given by C_4, C_3 and C_3', cmp. Fig. 1). The torsion angles τ for the equilibrium geometries of the ICT state computed in the equilibrium and non-equilibrium solvation limits differ by only $\approx 9°$. All other internal coordinates are for the two structures nearly the same (cmp. Table 2). The torsion angle of the amino group is, however, with $\tau = 65°$ (non-eq) and $\tau = 56°$ (eq) smaller than in the gas phase. Also the out-of-plane angle of the dimethyl-amino group in solution is with $\phi \approx 33°$ smaller than in the gas phase study. Similar as in the gas phase, we find also in solution besides the twisting of the dimethyl-amino group, an increase of the C≡N and the N–C_4 bond lengths accompanied by a shortening of the C_1–C bond length from ground to the excited state. *I.e.* the phenyl moiety shows in the ICT state a quinoidal distortion. This is an expected consequence of the charge transfer from the lone-pair of the amino group to the benzene ring. The dipole moment of the ICT minimum in both

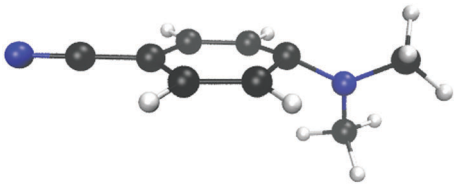


Fig. 3 Optimized geometry of the ICT state of DMABN at COSMO-RI-ADC(2)/def2-TZVPP level in the framework of post-SCF reaction field approach (non-equilibrium limit, ε = 36.7 and n^2 = 1.81).

This journal is © the Owner Societies 2018

Published on 20 April 2018. Downloaded by Ruhr Universitat Bochum on 1/16/2019 9:37:32 AM.

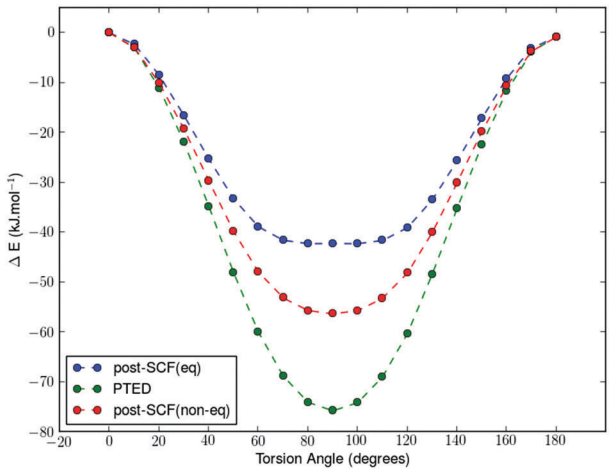


Fig. 4 Calculated potential energy curves for the ICT state of DMABN at the COSMO-ADC(2)/def2-TZVPP level as a function of the torsion angle τ. For further details see the text.

the equilibrium and the non-equilibrium solvation limits do not change much relative to the corresponding value for the ICT state at the Franck–Condon point (from 17.1 D to 17.5 D and 18.0 D, respectively).

To analyze the importance of state-specific reaction field contributions for the PES of charge transfer states we calculated unrelaxed PES scans for the ICT state of DMABN along the torsion angle defined by the atoms $C_{Me}NC_4C_3$ (cmp. Fig. 1) with all other internal coordinates constrained to their values in the PTE-COSMO-MP2 ground state geometry. The results for the equilibrium and non-equilibrium post-SCF and the PTED reaction field scheme from ref. 22 are shown in Fig. 4. For all three reaction field schemes increasing the torsion angle leads initially to a fast decrease in energy and agree well in the regime of $\pm 40^\circ$ around Franck–Condon point which is important for the short-time dynamics. For the post-SCF (eq) the potential reaches a flat minimum with a width of $\approx \pm 25^\circ$, while the post-SCF (noneq) and the PTED curves reach deeper sharp minima with essentially fully twisted geometries. Thus, an accurate description of the ICT minimum requires a reaction field scheme which includes a state-specific response to the excited state electron density. As pointed out above, such schemes are not suited for geometry optimization starting from the Franck–Condon point if one does not know that there will be no state intersections along the relaxation path on the excited state PES. DMABN, where S_1 and S_2 have, depending on the solvent polarity, an avoided crossing and/or conical intersection between the Franck–Condon point and the ICT or LE minimum, is a typical example for such a situation.

3.2 The 2-iodo-benzimidazolium·OTF ion pair in water

The 2-iodo-benzimidazolium·OTF ion pair is used as a second test system to study solvent effects on electronic excitation energies and geometries of excited states in solution. The Lewis acid character of the 2-iodo-benzimidazolium cation and the Lewis base character of the triflate anion lead in the ground state to the formation of a halogen-bonded 2-iodo-benzimidazolium·OTF complex. It is noteworthy that the solvent has significant effects on the geometry of the ion pair, in particular on the length of the halogen bond which shrinks in solution by ≈ 0.38 Å compared to the corresponding bond length in vacuum, as well as on the binding energy in the ground state where the structure with stacking interaction between the triflate anion and the five-membered ring is energetically more favored over the halogen-bonded structure by about 3.7 kcal mol^{-1}. We have investigated the vertical excitation energies and analyzed the natural transition orbitals for the three lowest transitions in vacuum and in aqueous solution. Water is usually the worst-case scenario for continuum solvation models. In vacuum, the first transition at 4.55 eV has a mixed inter- and intramolecular CT character (see the ESI† for the NTOs in the vacuum case). The second and third states in vacuum at 4.67 eV and 5.15 eV are, respectively, inter- and intramolecular CT transitions. Table 3 summarizes the excitation energies, transition moments and the changes of dipole moments with respect to the ground state obtained in vacuum and in aqueous solution within the post-SCF and PTED schemes.

Table 3 Calculated vertical excitation energies $\Delta\mathscr{G}$ (eV), transition moments f and the changes of dipole moments $\Delta\mu$ (D) for the first three electronic excited states of the halogen-bonded 2-iodo-benzimidazolium·OTF ion pair in vacuum and aqueous solution (in the non-equilibrium solvation limit, ε = 80.4 and n^2 = 1.78)[b]

	Reaction field		
	In vacuo	PTED	Post-SCF
$\Delta\mathscr{G}_{1,0}$	4.55	4.75	4.70
f_1	0.41	0.46	0.55
$\Delta\mu_1$[a]	−7.82	1.27	1.28
$\Delta\mathscr{G}_{2,0}$	4.67	5.15	5.17
f_2	0.08	0.08	0.13
$\Delta\mu_2$	−19.33	5.97	6.94
$\Delta\mathscr{G}_{3,0}$	5.15	5.61	5.64
f_3	0.00	0.00	0.00
$\Delta\mu_3$	−10.19	5.62	5.99

[a] $\Delta\mu_i = \mu_i - \mu_0$ with μ_0 as the dipole moment of the ground state. [b] All calculations are carried out at the COSMO-RI-ADC(2)/def2-TZVPP level using geometries optimized at the PTE-COSMO-MP2/def2-TZVPP level. Excited state energies are reported in different environments: '*in vacuo*' refers to the gas phase, for both PTED and post-SCF reaction field schemes water has been used as the solvent (post-SCF reaction field has been used in the non-equilibrium solvation limit, ε = 80.4 and n^2 = 1.78). The PTED calculations are equilibrated for the ground state and include state-specific excited state non-equilibrium corrections.

The characters of the excited states predicted by the post-SCF reaction field scheme for the three lowest states agree with those obtained with the more costly PTED scheme. Also the vertical excitation energies obtained with the two reaction field schemes are in good agreement. The results from the post-SCF scheme for the second and third states are only marginally higher by about 0.02 and 0.03 eV, respectively, and for the first excited state slightly lower by 0.05 eV. The values of the transition moments calculated in both approaches predict that in the UV spectrum of 2-iodo-benzimidazolium·OTF the first excited state is a bright state.

The stabilization of the local charges on the triflate anion and the benzimidazolium rings by the polar solvent and the corresponding weakening of the ionic interaction results in

Published on 20 April 2018. Downloaded by Ruhr Universitat Bochum on 1/16/2019 9:37:32 AM.

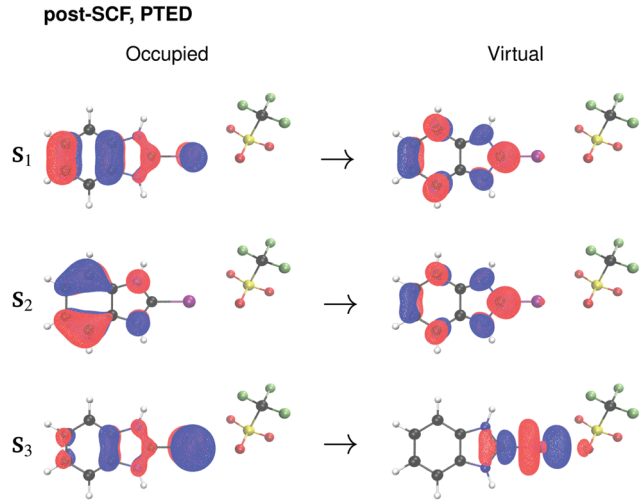


Fig. 5 Natural transition orbitals of 2-iodo-benzimidazolium·OTF calculated at COSMO-RI-ADC(2)/def2-TZVPP level within the post-SCF scheme (the same as for PTED) in aqueous solution (ε = 80.4 and n^2 = 1.78).

different characters for the electronic transitions in water compared to the vacuum case, especially for the second and third states. In accord with this, the values for the changes of the dipole moment upon excitation, $\Delta\mu$, predicted for these three states are negative in vacuum due to the decrease of the dipole moment in the excited states, while in aqueous solution both reaction field schemes predict positive values for $\Delta\mu$, *i.e.* an increase of the dipole moment upon excitation.

As shown in Fig. 5, both, the post-SCF and the PTED reaction field schemes, predict in aqueous solution a locally $\pi \rightarrow \pi^*$ excited character for the S_1 state with a small intramolecular CT from the iodine atom to the conjugated rings. Also they give with 5.17 eV (post-SCF) and 5.15 eV (PTED) very close excitation energies for the second excited state with $\pi \rightarrow \pi^*$ character and also agree well with 5.64 eV (post-SCF) and 5.61 eV (PTED) for the excitation energies of the third excited state with $n \rightarrow \sigma^*$ character (from a lone pair of the iodine atom to the σ^* orbital of the C–I bond).

Also for the 2-iodo-benzimidazolium·OTF ion pair we applied the newly developed gradient implementation for COSMO-RI-ADC(2) to determine the equilibrium geometry of the lowest singlet excited state S_1 using the def2-TZVPP basis set, Fig. 6.

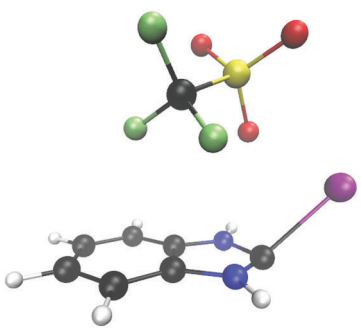


Fig. 6 The equilibrium structure of the S_1 state in aqueous solution at COSMO-RI-ADC(2)/def2-TZVPP level within the post-SCF reaction field scheme (non-equilibrium limit, ε^2 = 80.4 and n^2 = 1.78).

The striking difference between the S_1 and the S_0 equilibrium structures is that in the S_1 state the attraction between the CF_3 group and the π-system of the benzimidazolium rings dominates over the I–O halogen bond interaction. The charge transfer from the p_π orbital of iodine to the benzimidazolium gives rise to a C–I bond elongation by $\approx$0.4 Å and an out-of-plane bending of the C–I bond by $\approx 46^\circ$ similar as observed for the amino group in the ICT state of DMABN.

4 Summary and conclusions

In this work we applied a post-SCF reaction field scheme, which is intermediate between the PTE and PTED reaction field schemes, for combining the COSMO polarizable continuum model with the correlated wavefunction method ADC(2) for calculations on electronically excited states including solvent effects. The theory for analytic excited state gradients for the post-SCF variant of COSMO-ADC(2) has been derived and implemented for equilibrium and non-equilibrium situations so that solvent effects on excited state relaxation dynamics, equilibrium geometries and potential energy surfaces can be studied at this level of theory. The post-SCF reaction field scheme goes beyond PTE by including linear response contributions to the reaction field at the correlated, *i.e.* here the ADC(2) level, but it avoids perturbative corrections and waives the state-specific self-consistent construction of the reaction field for the excited states of the PTED scheme. Both would prevent a qualitative correct description of avoided crossings and conical intersections of the excited states and the PTED scheme would increase the computational costs by a large factor and diminish the numerical stability of the molecular gradients. With the post-SCF reaction field scheme the additional computational costs for including solvent effects at the correlated wavefunction level on excitation energies and excited state molecular gradients are only a small fraction of the costs for the corresponding gas phase calculation.

We demonstrated the capability of COSMO-RI-ADC(2) to provide solvent-induced shifts for UV spectra and excited state equilibrium structures within the post-SCF scheme for two different compounds: DMABN and 2-iodo-benzimidazolium·OTF. Although in the first case we observe an inversion in the order of the lowest two excited states between the post-SCF and the PTED scheme in acetonitrile solution where the two states are very close in energy, the two reaction field schemes agree in general well for solvent shifts of excitation energies, transition and dipole moments. For both sample applications we investigated the relaxation of the excited state structures for the first singlet excited states starting from the Franck–Condon geometries at the COSMO-RI-ADC(2) level of theory within the post-SCF scheme.

In conclusion, COSMO-RI-ADC(2) with the post-SCF reaction field scheme with its consistent description of the excited state PES, which are obtained from a common eigenvalue problem, is a highly attractive method to calculate not only vertical excitation energies but also properties related to the PES like

 This journal is © the Owner Societies 2018

Published on 20 April 2018. Downloaded by Ruhr Universitat Bochum on 1/16/2019 9:37:32 AM.

equilibrium geometries, deexcitation pathways and Stoke shifts in solution beyond the TDDFT level. The implementation of analytic excited state gradients for this approach provides the possibility to obtain useful insights into photophysical properties and photochemical pathways in solution at the correlated wavefunction level. The price that is paid to obtain PES which retain a physically correct structure in the vicinity of (near) degeneracies is the exclusion of state-specific corrections that account for changes of the reaction field induced by the change of density upon excitation is a limited applicability for states with large charge transfer. This is a dilemma for reaction field methods which is difficult to resolve.

The reported COSMO-RI-ADC(2) functionalities have been implemented in a development version of the TURBOMOLE program package[29,30] and will be made available in forthcoming releases of the package.

Conflicts of interest

There are no conflicts to declare.

Acknowledgements

We gratefully acknowledge financial support from the Cluster of Excellence RESOLV (EXC 1069) and project Ha 2588/8-1 funded by the Deutsche Forschungsgemeinschaft.

References

1 J. Tomasi, B. Mennucci and R. Cammi, *Chem. Rev.*, 2005, **105**, 2999–3093.
2 C. Cramer and D. Truhlar, *Chem. Rev.*, 1999, **99**, 2161–2200.
3 A. Klamt, *Wiley Interdiscip. Rev.: Comput. Mol. Sci.*, 2011, **1**, 699–709.
4 A. Klamt, *J. Phys. Chem.*, 1996, **100**, 3349–3353.
5 J. Tomasi, B. Mennucci and R. Cammi, *Chem. Rev.*, 2005, **105**, 2999–3094.
6 B. Mennucci, *Wiley Interdiscip. Rev.: Comput. Mol. Sci.*, 2012, **2**, 386–404.
7 R. Cammi, B. Mennucci and J. Tomasi, *J. Phys. Chem. A*, 2000, **104**, 5631–5637.
8 M. Cossi and V. Barone, *J. Chem. Phys.*, 2001, **115**, 4708–4717.
9 G. Scalmani, M. J. Frisch, B. Mennucci, J. Tomasi, R. Cammi and V. Barone, *J. Chem. Phys.*, 2006, **124**, 094107.
10 R. Cammi, *J. Chem. Phys.*, 2009, **131**, 164104.
11 R. Cammi, *Int. J. Quantum Chem.*, 2010, **110**, 3040–3052.
12 R. Cammi, *Int. J. Quantum Chem.*, 2012, **112**, 2547–2560.
13 M. Caricato, *J. Chem. Theory Comput.*, 2012, **8**, 5081–5091.
14 S. Yomosa, *J. Phys. Soc. Jpn.*, 1974, **36**, 1655.
15 B. Mennucci, R. Cammi and J. Tomasi, *J. Chem. Phys.*, 1998, **109**, 2798–2807.
16 K. V. Mikkelsen, P. Jrrgensen and H. J. A. Jensen, *J. Chem. Phys.*, 1994, **100**, 6597–6607.
17 O. Christiansen, T. Nymand and K. V. Mikkelsen, *J. Chem. Phys.*, 2000, **113**, 8101–8112.
18 R. Cammi, S. Corni, B. Mennucci and J. Tomasi, *J. Chem. Phys.*, 2005, **122**, 104513.
19 S. Corni, R. Cammi, B. Mennucci and J. Tomasi, *J. Chem. Phys.*, 2005, **123**, 134512.
20 R. Improta, V. Barone, G. Scalmani and M. J. Frisch, *J. Chem. Phys.*, 2006, **125**, 054103.
21 M. Caricato, B. Mennucci, J. Tomasi, F. Ingrosso, S. Corni and G. Scalmani, *J. Chem. Phys.*, 2006, **124**, 124520.
22 B. Lunkenheimer and A. Köhn, *J. Chem. Theory Comput.*, 2013, **9**, 977–994.
23 O. Christiansen and K. V. Mikkelsen, *J. Chem. Phys.*, 1999, **110**, 8348.
24 R. Cammi, *J. Chem. Phys.*, 2009, **131**, 164104.
25 M. Caricato, *J. Chem. Phys.*, 2011, **135**, 074113.
26 A. Klamt and G. Schüürmann, *J. Chem. Soc., Perkin Trans. 2*, 1993, 799–805.
27 J. Schirmer, *Phys. Rev. A: At., Mol., Opt. Phys.*, 1982, **26**, 2395–2416.
28 C. Hättig and F. Weigend, *J. Chem. Phys.*, 2000, **113**, 5154–5161.
29 TURBOMOLE V7.2 2017, a development of University of Karlsruhe and Forschungszentrum Karlsruhe GmbH, 1989–2007, TURBOMOLE GmbH, since 2007, available from http://www.turbomole.com.
30 F. Furche, R. Ahlrichs, C. Hättig, W. Klopper, M. Sierka and F. Weigend, *Wiley Interdiscip. Rev.: Comput. Mol. Sci.*, 2014, **4**, 91–100.
31 T. Schwabe, K. Sneskov, J. M. H. Olsen, J. Kongsted, O. Christiansen and C. Hättig, *J. Chem. Theory Comput.*, 2012, **8**, 3274–3283.
32 M. Head-Gordon, R. J. Rico, M. Oumi and T. J. Lee, *Chem. Phys. Lett.*, 1994, **219**, 21–29.
33 O. Christiansen, H. Koch and P. Jørgensen, *Chem. Phys. Lett.*, 1995, **243**, 409–418.
34 C. Hättig, *Adv. Quantum Chem.*, 2005, **50**, 37–60.
35 D. Hrsak, A. M. Khah, O. Christiansen and C. Hättig, *J. Chem. Theory Comput.*, 2015, **11**, 3669–3678.
36 K. Sneskov, T. Schwabe, J. Kongsted and O. Christiansen, *J. Chem. Phys.*, 2011, **134**, 104108.
37 F. Weigend and R. Ahlrichs, *Phys. Chem. Chem. Phys.*, 2005, **7**, 3297–3305.
38 A. Hellweg, C. Hättig, S. Höfener and W. Klopper, *Theor. Chem. Acc.*, 2007, **117**, 587–597.
39 I. Georgieva, A. J. A. Aquino, F. Plasser, N. Trendafilova, A. Köhn and H. Lischka, *J. Phys. Chem. A*, 2015, **119**, 6232–6243.
40 N. Dozova, R. Kumar, T. Pradhan, F. Lacombat, B. Valeur, J. S. Kim and P. Plaza, *Chem. Commun.*, 2015, **51**, 14859–14861.
41 B. F. E. Curchod, A. Sisto and T. J. Martínez, *J. Phys. Chem. A*, 2017, **121**, 265–276.
42 K. A. Zachariasse, M. Grobys and E. Tauer, *Chem. Phys. Lett.*, 1997, **274**, 372–382.
43 S. I. Druzhinin, N. P. Ernsting, S. A. Kovalenko, L. P. Lustres, T. A. Senyushkima and K. A. Zachariasse, *J. Phys. Chem. A*, 2006, **110**, 2955–2969.
44 V. A. Galievsky and K. A. Zachariasse, *Acta Phys. Pol., A*, 2007, **112**, S39–S56.
45 A. Köhn and C. Hättig, *J. Am. Chem. Soc.*, 2004, **126**, 7399–7410.
46 C. Hättig, A. Hellweg and A. Köhn, *J. Am. Chem. Soc.*, 2006, **128**, 15672–15682.